institut de physique nucléaire
LABORATOIRE ASSOCIÉ A L'IN2P3

IPNO DRE 83-26

Valence and inner proton hole states in ^{207}Tl via the (d,^{3}He) réaction at 108 MeV.

H. LANGEVIN-JOLIOT, E. GERLIC, J. GUILLOT
and J. VAN De WIELE,

Institut de Physique Nucléaire, B.P. n°1,
91406 Orsay (France)

UNIVERSITÉ PARIS SUD

IPNO DRE 85-26

Valence and inner proton hole states in ^{207}Tl via the (d,^{3}He) réaction at 108 MeV.

H. LANGEVIN-JOLIOT, E. GERLIC, J. GUILLOT
and J. VAN De WIELE,

Institut de Physique Nucléaire, B.P. n°1,
91406 Orsay (France)

VALENCE AND INNER PROTON HOLE STATES IN ^{207}Tℓ VIA THE (d,^{3}He) REACTION AT 108 MeV.

H. Langevin-Joliot, E. Gerlic, J. Guillot
and J. Van de Wiele,
Institut de Physique Nucléaire, B.P. n° 1,
91406 Orsay (France)

* * *

ABSTRACT

The excitation energy spectra of the residual nucleus ^{207}Tℓ have been investigated up to 14 MeV using the (d,^{3}He) reaction at 108 MeV. New groups and high lying structures are first observed up to 8.3 MeV, in addition to the five known low lying levels. Beyond a minimum at 7.13 MeV, weaker structures are observed riding over an asymetric bump located around 9 MeV. DWBA analysis of angular distributions have allowed ℓ attributions and the determination of valence and inner hole spectroscopic factors. It is found that the valence levels at 1.33 MeV, 1.67 MeV, and 3.47 MeV exhaust respectively about 65%, 60% and 45% of the $1h_{11/2}$, $2d_{5/2}$ and $1g_{7/2}$ sum rules. The missing strengths are found below 8.3 MeV. The $2d_{5/2}$ and $1g_{7/2}$ holes contribute mainly to some well

concentrated groups, whereas the $1h_{11/2}$ strength is distributed more smoothly. Small contributions of $1g_{9/2}$ and 2p strengths are tentatively identified below 7.13 MeV. The highest lying energy region up to 14 MeV may approximately account for the $1g_{9/2}$ and $(1f_{5/2})$ total sum-rule and about 70% of the 2p strength. The $1g_{9/2}$ strength gives the largest contribution to the asymetric bump around 9 MeV. The deduced experimental strength functions are compared with theoretical calculations.

NUCLEAR REACTION : $^{208}Pb(d,^{3}He)E = 108$ MeV, measured $\sigma(E_{^{3}He}, \theta)$, ^{207}Tl deduced levels and structures, E_x, ℓ, C^2S ; DWBA analysis ; valence, inner proton holes.

I - INTRODUCTION

While neutron pick-up reactions[1] have been rather extensively used to study both valence and more deeply bound neutron hole states, the experimental status concerning proton hole states is much less satisfying. This may be related with the rather restricted choice of nuclear reactions induced by light projectiles which populate protons hole states, that is the $(d,^3He)$ reaction and the (t,α) reaction. Moreover, only tritons of maximum incident energies around 20 MeV are available up to now. The recent study of deeply bound proton hole states have concentrated mainly on Zr and Sm targets, using the $(d,^3He)$ reaction at 52 MeV[2].

Among the heavy nuclei, ^{208}Pb offers a unique opportunity to investigate single hole (or particle) states in a doubly closed shell nucleus. Up to now, most pick-up experiments have only measured the ^{207}Tl excitation energy spectra up to 2 MeV or 4 MeV for the more complete ones[3-5]. Under these conditions, a significant part of the $1h_{11/2}$, $2d_{5/2}$ and especially of the higher-lying $1g_{7/2}$ valence hole strengths were not observed. Moreover, the spectroscopic factors deduced by the different authors for the main $11/2^-$ and $7/2^+$ valence fragments are not in good agreement.

We present in this paper a study of the reaction $^{208}Pb(d,^3He)^{207}Tl$ at the incident energy of 108.4 MeV. This energy is larger than those used in all previous experiments and more suitable to enhance the cross-sections corresponding to the large angular momentum transfers, such as $l = 5$ and particularly $l = 4$, over a large excitation energy range (0.-8.MeV). We have investigated the residual ^{207}Tl spectra up to 14 MeV excitation energy to search for the deep $1g_{9/2}$ hole strength, in addition to the missing $1h_{11/2}$, $2d_{5/2}$ and $1g_{7/2}$ valence strengths.

II - EXPERIMENTAL SET-UP AND DATA REDUCTION

The experiment was performed with the 108.4 MeV deuteron beam of the Orsay synchrocyclotron, using the achromatic line facility coupled

to the large "Montpellier" spectrometer. The detection system consisted of two multiwire chambers and two plastic scintillators coupled to photomultipliers. The two localisation chambers achieved a good determination of the position and angle of the trajectory at the focal plane. The plastic scintillators provided energy loss signals thus allowing the clean separation of ^{3}He particles from the background of protons, deuterons, tritons and alpha particles. The targets were self-supported foils of enriched ^{208}Pb (97.8%). The achieved energy resolutions, respectively 150 keV and 250 keV for the low lying levels and the newly investigated high excitation energy region, mainly result from the target thicknesses (5.8 mg/cm^2 and 10 mg/cm^2). Two settings of the magnetic field were used to study the 2.5 - 14 MeV energy range. Angular distributions were taken from 4° to 18° in typically 2° steps (1° for the low lying levels).

A Mylar target was also studied to allow the comparison with the contaminant peaks of the ^{207}Tl spectra.

A typical experimental spectrum obtained at 8° is presented on fig. 1. The first low lying levels $1/2^+$, $3/2^+$, $11/2^-$, $5/2^+$ are all rather strongly excited, especially the $11/2^-$ level, which was not the case in the previous experiments at smaller incident energies. But the reaction is not a strongly selective as for example the (^{3}He, α) reaction at 101 MeV[6], and the $\ell = 0$ and moreover $\ell = 2$ transfers are quite well observed.

The fragment of the $1g_{7/2}$ subshell already observed at 3.47 MeV, dominates the next part of the spectrum which extends up to a minimum at 7.3 MeV. In this region, rather strong groups point at 4.0 MeV, 4.55 MeV, 4.95 MeV and 5.8 MeV and smaller ones at 2.74 MeV, 6.2 MeV, 6.8 MeV. Beyond the minimum at 7.13 MeV which is located in the region of the proton and neutron emission thresholds, the spectrum exhibits a large asymetric bump with its flat maximum around 9 MeV. Weak structures riding on it are identified at 7.4 MeV, 7.75 MeV and 8.05 MeV ; beyond 8.3 MeV, the cross-section decreases smoothly up to the highest measured energy.

The contaminant ^{16}O and ^{12}C at the surface of the target, give splitted peaks which have been subtracted, using the result of the mylar target.

The rapidly increasing density of levels with excitation energy in ^{207}Tl combines with the experimental energy resolution to merge the many individual peaks into groups or structures, far below the neutron and proton thresholds. In order to extract the cross section data, the spectra were thus separated into energy slices, as shown on fig. 1. In addition, in order to characterize the groups between 3.5 and 8.3 MeV more easily, the corresponding slices were divided into a "structure" part and an underlying part changing more smoothly with excitation energy. This was achieved in a systematic way at each angle by using straight lines joining the points at 80% of the cross section measured at the lower minima (see fig. 1).

III - ANGULAR DISTRIBUTIONS AND DWBA ANALYSIS

A) The low lying levels

The angular distributions of the well known $1/2^+$, $3/2^+$, $11/2^-$, $5/2^+$ and $7/2^+$ levels respectively at 0.0, 0.35, 1.33, 1.67 and 3.47 MeV are presented in fig. 2. The results were analysed in the framework of the usual zero range distorted wave Born approximation, without any radial cut-off.

We tried different optical potentials available in the literature in the proper energy range. For the entrance channel, the best fits are obtained with the deuteron potential[7] deduced by fitting elastic scattering data at 108 MeV with a potential of the type proposed by Daenick[8]. The calculated shapes are found to depend much more on the ^3He exit channel. In particular, we point out that the usual ^3He potential with a pure volume imaginary term[9], which reproduces very well elastic scattering angular distributions and successfully describes inelastic scattering data[10] and (^3He, α) pick-up data at 101 MeV[6], fails completely in the present case (see fig. 2- set C). Pure surface imaginary potentials

have also been used in the analysis of ^{3}He elastic scattering data[9,11]. The parameter set A (table 1) corresponding to such a choice could reasonably reproduce the angular distribution shapes, as shown on fig. 2. The deduced spectroscopic factors (see table 2) are however very small compared to the sum rules, even for the first $2d_{3/2}$ first level, which is well known as a nearly pure shell model state. More interesting is parameter set B that we have built up as a "break-up type" potential by adding a proton potential[12] and a deuteron potential[8] corresponding respectively to 35 MeV and 75 MeV incident energy. Such a procedure has already been successfully used to describe neutron pick-up reactions with high energy complex particles in the exit channel[1]. The "break-up" potential set B, involving both volume and surface absorption, reproduces fairly well elastic scattering results and gives the best fits to the present (d,^{3}He) angular distributions, as shown in fig. 2. Moreover, it reproduces well the expected strong concentration of the $d_{3/2}$ strength in the 0.35 MeV level.

The spectroscopic factors deduced in the present work have been obtained using a standard form factor (table 1) and the usual expression $C^2S = \frac{2j+1}{2.95} \sigma_{exp}/\sigma_{DW}^{lj}$. They are compared in table 2 with previous results. With the choice of parameter set B, all measurements of the $d_{3/2}$ and $d_{5/2}$ spectroscopic factors are in reasonable agreement, the first $d_{3/2}$ level exhausting nearly the full strength, whereas the $d_{5/2}$ level contributes for about 60% of the corresponding sum rule only. The situation is more conflicting as concerns the $h_{11/2}$ and $g_{7/2}$ levels. We find respectively 65% and 45% of the corresponding total proton hole strengths only. One may notice that taking the $d_{3/2}$ level as a reference, the relative values deduced with the parameter set A would even give somewhat smaller percentages of the sum rules. It should be recalled that angular distribution shapes and relative spectroscopic factors do not much depend on the form factor radius (whereas with a 1% smaller radius, absolute values become about 10% larger). The $h_{11/2}$ and $g_{7/2}$ level spectroscopic factors respectively increases and decreases by 10% and 14% if the spin orbit parameter λ is taken as 15 instead of 25. This last standard value has also been adopted in the analysis of subcoulomb transfer reaction (t,α) in order to determine orbit radii in ^{207}Tl[13].

Summerizing the results and discussion, we conclude that significant parts of the $d_{5/2}$, $h_{11/2}$, $g_{7/2}$ strengths are missing in the well known low lying levels and have to be searched for in a larger excitation energy range.

8) The excitation energy region between 2.5 and 8.3 MeV

As indicated previously, this region is characterized by many groups or structures ; the upper part (structures) and the underlying part of each energy slice have been analysed separately.

The angular distributions of the groups presented on fig. 3(a), 3(b) may reasonably be described by the significant contributions of two ℓ transfers at most. As the first $2d_{3/2}$ level already exhausts nearly all the corresponding strength, all $\ell = 2$ fragments have been attributed to the $2d_{5/2}$ strength. The $\ell = 4$ fragments up to 5.4 MeV have been attributed to the $1g_{7/2}$ strength, as discussed later on.

Four groups exhibit pure (structure M at 8.05 MeV) or nearly pure $\ell = 4$ (+ $\ell = 2$) angular distributions (groups B at 3.05 MeV, D at 4.0 MeV and H at 5.8 MeV). Two other groups are also identified $\ell = 4 + \ell = 2$, with larger relative amounts of $d_{5/2}$ strength (30% for the group F at 4.95 MeV, which is the most excited in this structure region). One notices that small percentages of the $\ell = 2$ strength are rather easily identified over the dominant $g_{7/2}$ strength, due to their comparatively larger cross sections, especially at small angles (4°-6°).

The $2d_{5/2}$ strength is found to be the main component of the three structures E at 4.55 MeV, and J and K at 6.8 and 7.38 MeV. None of the structure exhibits pure or nearly pure $\ell = 5$ angular distribution. The largest strength concentration is found in structure E (with about 2% of the sum rule limit). The weak structure L angular distribution exhibits rapidly increasing cross sections at forward angles, with the maximum beyond 4° that are characteristic of $\ell = 1$ (in addition to the dominant $\ell = 4$ contribution). Since DWBA predictions are rather similar for $p_{1/2}$ and $p_{3/2}$ hole, mean 2p strength percentages are determined. The weak

G and I structure angular distributions can not be explained with the main contributions of two ℓ components only.

The angular distributions of the underlying part of the different energy slices have common features, as shown on fig. 4(a). The behaviour at small angles cannot be reproduced without contributions of both $\ell = 1$ and $\ell = 2$ transfers, whereas at larger angles it implies contributions of larger ℓ, mainly $1h_{11/2}$ (or $1g_{9/2}$ in the case of slices K-L-M around 8 MeV).

The results concerning absolute hole strengths are summerized in table III. The spectroscopic factors corresponding to the "structure" and underlying parts of each energy slice have been extracted, and then summed up. These factors are generally small (one to few percent of the corresponding strengths) with the exception on those of the slices D and F which respectively exhaust 13% and 17% of the $1g_{7/2}$ strength. Uncertainties in the experimental angular distribution decompositions are larger for the spectrum underlying parts than for the structures, especially if four different ℓ values contribute significantly. It should however be noticed that large errors (30% to 50%) eventually associated with the smallest component strengths in each slice, do not give large effects on the summed spectroscopic strengths reported in table 3.

The behaviour of the $1g_{7/2}$, $2d_{5/2}$, $1h_{11/2}$ strength distributions is quite different, most of the $1g_{7/2}$ and $2d_{5/2}$ strengths being concentrated in the "structure" part of the spectra, while the $1h_{11/2}$ strength is mostly distributed smoothly in the underlying part of the spectra, as shown in table III.

The valence hole strengths are found mainly concentrated up to the minimum at 7.13 MeV excitation energy. With the assumption that all $\ell = 4$ fragments above 5.5 MeV are $1g_{9/2}$, the percentages of the sum rules achieved for the valence $1h_{11/2}$, $2d_{5/2}$ and $1g_{7/2}$ proton hole states up to 7.13 MeV reach nearly 90%.

c) The high excitation energy region (8.3 - 14 MeV)

No structure could be clearly identified beyond 8.3 MeV excitation energy. The ^{11}B contaminant peak blurred up a small peaking observed at some angles at 8.65 MeV. Typical angular distributions obtained for some of the total energy slices are presented in fig. 4(b) together with tentative decompositions into several ℓ components of the inner shells. In all the energy region, the behaviour at small angles is characteristic of rather large 2p contributions, and the maximum or shoulder near 10° corresponds mainly to contributions of the $1g_{9/2}$ strength. Even large percentages of the $1f_{5/2}$ strength are rather difficult to identify without ambiguity, due to the small cross section for the same percentage of strength compared to $1g_{9/2}$. Moreover the $1f_{5/2}$ maximum would just fill in the minimum of the 2p angular distribution : the resulting decomposition thus depends critically on the assumed 2p angular distribution shape ; the calculated DWBA curves cannot in this case be checked against well known 2p experimental distributions. In fact, the predicted curves exhibit very deep minima, which seems unrealistic. Any significant fragment of the 2p strength would have induced drastic effects on the complex angular distributions. It has thus seemed to us reasonable to smooth out the minima of the 2p curves ; even with this procedure, the deduced 2p strength between 8.3 MeV and 14 MeV, only amounts to 55% of the sum rule.

At the largest angles, we find it impossible to fit the cross sections, obtained without any subtraction of a background. This may indicate some contribution of other processes. The spectroscopic factors summerized in table III have thus to be considered as upper values.

IV - FRAGMENTATION OF VALENCE AND INNER HOLE STRENGTHS

The collective 3^- state at 2.63 MeV in ^{208}Pb, leads to one hole - one phonon configurations in ^{207}Tl which may strongly couple with valence hole configurations. The $(h_{11/2} \otimes 3^-)$ $5/2^+$ and $7/2^+$ configurations coupled to the $2d_{5/2}$ and $1g_{7/2}$ holes were considered to be the most important by

Hamamoto[14], and were expected to take away significant parts of these hole strengths into the region of 3 - 5 MeV excitation energy. The present experimental results support this conclusion ; the fragmentation is not only observed for the $2d_{5/2}$ and $1g_{7/2}$ hole but also for the $1h_{11/2}$ hole, and it is found to be much more important than predicted. More refined calculations of the spreading of valence and inner proton hole strengths in ^{207}Tℓ have recently been developped, using two different approachs[15,16].

Soloviev et al.[15] start with a description in term of quasi-particles in a Wood-Saxon well and introduce the coupling with one and two phonons of electric and magnetic type. Pham van Thieu et al.[16] develop a full calculation of the spreading of hole and particle states induced by the coupling of Hartree-Fock states to the collective excitation of the core ; the calculation is done using the effective force Skyrme III. Small artificial widths are introduced in both cases to build up strength functions which may describe the many levels with small pieces of the strength.

Our experimental results concerning the valence dominant fragments, and the centroïds and widths of the observed valence and inner hole strengths are summerized in table IV and compared with relevant theoretical values.

A) The valence hole strength

The ground state $1/2^+$ and the first $3/2^+$ level at 0.35 MeV are found to exhaust respectively nearly all the $3s_{1/2}$ and $2d_{3/2}$ strengths, in agreement with the theoretical expectations of ref. 15 and ref. 16. Both calculations overestimate the strengths of the $1h_{11/2}$ level at 1.33 MeV and that of the $2d_{5/2}$ level at 1.67 MeV by about 25% as compared to our experimental values. The strength given in ref. 16 for the $1g_{7/2}$ level at 3.47 MeV agrees with the experimental result, whereas the value of ref. 15 is too large. The positions of the dominant fragment of each valence hole states are reasonably well predicted by the quasi-particle-phonon calculation of ref. 15. The separation energies determined in

ref. 16 depend on the calculated Hartree-Fock energies ; in this case, the level spacing cannot be reproduced in detail.

The hole states nearest to the Fermi surface $3s_{1/2}$, $2d_{3/2}$, $1h_{11/2}$, $2d_{5/2}$, have as a common feature that a large amount of their strength is concentrated in one level whereas all other corresponding levels exhaust individually very small pieces of these strengths, at much higher excitation energies. The furthest valence $1g_{7/2}$ hole is distributed mainly among three levels or well located groups, up to 5.4 MeV, and in the underlying part of the spectra.

The largest part of the strength missing in the first $1h_{11/2}$ level is distributed rather smoothly from 3 to about 8 MeV excitation energy. The centroïd and width are found respectively at 6.0 and 2.8 MeV, the values deduced of ref. 16 being significantly smaller. As shown in table IV, the experimental centroïd of the total (about 95%) strength is located 1.5 MeV above the first fragment instead of 0.33 MeV as predicted.

The fragmentation of the $2d_{5/2}$ and $1g_{7/2}$ strengths deduced experimentally are compared in fig. 5. with the predictions of ref. 16. Each experimental energy scale has been shifted to bring the experimental and calculated main fragments at the same position. The general features of the experimental results are rather well reproduced.

Both experimental and theoretical $2d_{5/2}$ distributions present a broad (2.3 MeV width) concentration of strength, the centroïd of which is located 3.5 MeV above the first fragment ; the agreement is less good if one considers the total strength distribution, as shown in table IV. Due to the larger relative strength in the first fragment, the calculated centroïd is only shifted 0.7 MeV above this fragment, as compared to the observed value of about 1.4 MeV.

The calculation[16] reproduces the $1g_{7/2}$ strength concentration in a few fragments. We do not observe so much strength as calculated on the low energy side of the dominant fragment. The total experimental spreading width (taken for the strength up to 5.4 MeV excitation energy)

is smaller than the theoretical expectation (see table IV). However, the calculations strongly suggest that the experimental $\ell = 4$ strength observed above 5.4 MeV should indeed be attributed to $1g_{9/2}$ rather than to $1g_{7/2}$.

The general features of the $1g_{7/2}$ fragmentation calculated in ref. 15, do not agree with the present results ; the strength is too much concentrated in the first level, the residual strength being mainly located about 1.5 MeV higher.

A) The inner hole strengths

The experimental results concerning the inner hole states $1g_{9/2}$ (and 2p and moreover $1f_{5/2}$) are more qualitative. As shown in table IV, the $1g_{9/2}$ and $(1f_{5/2})$ strengths observed up to 14 MeV may exhaust the corresponding sum rules, whereas some 2p strength seems missing.

The experimental spreading of the $1g_{9/2}$ hole strength is compared in fig. 6, with the predictions of Soloviev et al.[15]. The energy scales are shifted by 1.25 MeV in order to emphazize the common features. In particular, the calculated strength function exhibits a small concentration of strength at low excitation energy, which may well be identified with the experimental maximum near 5.8 MeV, followed by the minimum at about 7 MeV. The three main peaks of the theoretical curve are then located in the region of the flat maximum of the experimental strength distribution. The total strength measured within 5 MeV in this region compares well with the predictions. However, the experimental curve is much smoother than the calculated one, and decreases very slowly toward high excitation energies. We emphazize that any strong concentration of the $1g_{9/2}$ strength ($\sim$ 30% within 0.75 MeV, as expected from the calculation) would have given a pronounced bump in the spectra. The total strength centroïd is well reproduced by the calculation of Pham et al.[16], as shown in table IV. However as two phonons components are not included in this calculation, a comparison of the spreading at high excitation energies would not be relevant.

The present experiment at high incident energy is not the best suited to study the 2p strength, which is found widely spread from 4 to 14 MeV (the highest studied excitation energy). The mean 2p strength function deduced from the calculation of Soloviev et al.[15] is spread over 10 MeV, but it exhibits two main maxima which have not been identified experimentally. An expected 10% to 15% amount of the 2p strength in an energy slice of 0.5 MeV, would have given obvious effects on the angular distribution (unless the 2p DWBA angular distribution has a very different shape than assumed). In the region of excitation energy up to about 6 MeV, the contribution of the $2d_{5/2}$ fragments to the cross sections hinders the determination of small fragments of the 2p strength.

As previously indicated, the $1f_{5/2}$ strength is the most difficult to identify. Thus, the values given in table IV for the centroïd and width are tentative only.

V - SUMMARY AND CONCLUSIONS

The present study of the $(d,^3He)$ reaction on ^{208}Pb, performed with the highest energy projectiles as compared to previous experiments, allows the observation of new features concerning the valence hole states and gives first evidence for the location of inner hole states in ^{207}Tl, especially $1g_{9/2}$. The experimental spectra exhibit a number of new groups or structures up to 8.3 MeV excitation energy, in addition to the five well known low lying levels. Beyond 7.13 MeV, the structures are observed over a smooth asymetric bump, the flat maximum of which is located around 9 MeV.

A striking feature of the results, as deduced from the DWBA analysis, is the overlapp of large parts of different valence and inner sub-shell components in the regions of excitation energy 2.5 - 7.13 MeV and 7.13 - 14 MeV respectively. The total $1h_{11/2}$, $2d_{5/2}$ and $1g_{7/2}$ strengths are far from being concentrated in the first $11/2^-$ and $5/2^+$ levels and in the $7/2^+$ level at 3.47 MeV. We find that a large part of the missing $2d_{5/2}$ strength is exhausted by some of the well located groups up to 5.4 MeV whereas the missing $1h_{11/2}$ strength seems to be more widely

spread among very many fragments. The missing $1g_{7/2}$ strength is found mainly concentrated between 2.5 and 5.4 MeV, especially within two new groups (at $\sim$ 4.0 and $\sim$ 4.95 MeV). With the assumption that all $\ell = 4$ fragments above 5.4 MeV are $1g_{9/2}$, the $1h_{11/2}$, $2d_{5/2}$ and $1g_{7/2}$ strengths measured up to 8.3 MeV account for about 90% of the sum rule typically.

About 10% of the $1g_{9/2}$ strength and 5% of the 2p strengths are tentatively identified below 7.13 MeV excitation energy. These strengths are found mainly concentrated in the next region between 7.13 MeV and 14 MeV ; this seems also to be the case of the $1f_{5/2}$ strength.

The present experimental results concerning the valence and inner hole strength distributions, have been compared with two recent theoretical predictions. The comparison is encouraging, although these calculations do not reproduce well, either the spreading of the valence $1g_{7/2}$ strength or that of the higher lying inner hole $1g_{9/2}$ strength, for example.

Further experiments with other reactions or incident energies would be useful, especially to better settle the contributions of the different inner hole states. Improved analysis and better comparison between experimental and theoretical results would also benefit to a more precise knowledge of widely spread strength distributions. In particular, consistent predictions of the fragment distribution as a function of excitation energy and of the corresponding form factor behaviour are highly desirable.

Further theoretical efforts are also needed to achieve a better understanding of the strong fragmentation of the valence and inner holes in heavy nuclei.

ACKNOWLEGMENT

The authors would like to thank the synchrocyclotron crew for the good running of the accelerator, and F. Reide and G. Chesneau for their help concerning the wire chamber operation and the electronic set-up. We thank V.G. Soloviev, Pham Van Thieu and N.V. Giai for communication of their results before publication, and for fruitful discussions.

REFERENCES

1) S. Galès, Nucl. Phys. A354 (1981) 193c and references therein
H. Langevin-Joliot et al., Phys. Lett. 114B (1982) 103 and references therein

2) P. Doll et al., Phys. Lett. 82B (1979) 357
A. Stuirbrink et al., Z. Physics A, Atoms and Nuclei, 297 (1980) 307

3) D. Royer et al., Nucl. Phys. A158 (1970) 516

4) P.D. Barnès, E.R. Flynn, G.J. Igo and D.D. Amstrong, Phys. Rev. C1 (1970) 228

5) E.R. Flynn et al., Nucl. Phys. A279 (1977) 394

6) J. Guillot et al., Phys. Rev. C21 (1980) 879

7) C. Djalali, Thesis, (1981) Orsay

8) W.W. Daehnick, J.D. Childs and Z. Vrcelj, Phys. Rev. C21 (1980) 2253

9) A. Djaloeis, J.P. Didelez, A. Galonsky and W. Oelert, Nucl. Phys. A306 (1978) 221

10) D. Lebrun, Thesis (1981), Grenoble

11) C.B. Fulmer, J.C. Hafele and N.M. Clarke, Phys. Rev. C12 (1975) 87

12) W.T.H. Van Oers et al., Phys. Rev. C10 (1974) 307

13) P.W. Woods et al., Phys. Lett. 116B (1982) 320

14) I. Hamamoto, Physics Reports 10 (1974) 63

15) V.G. Soloviev, Ch. Stoyanov, and V.V. Voronov, to be published

16) Pham Van Thieu and N. Van Giai, to be published

FIGURE CAPTIONS

Fig. 1 : Typical excitation energy spectrum observed in the reaction $^{208}Pb(d,^{3}He)^{207}Tl$ at 108 MeV. The broken line devides each energy slice into a "structure" part and a residual part - S_n, S_p are the neutron and proton separation energies.

Fig. 2 : Angular distribution of the valence main fragments. The curves are DWBA predictions using different sets of optical potentials. Set A-broken line. Set B-continuous line. Set C-usual volume potentiel[9] - dotted lines (see text).

Fig. 3 : Angular distribution of groups and structures in the 2.5-8.3 MeV region - The cross sections correspond to the "structure" part of energy slices labelled in fig. 1. The curves are DWBA calculations with pure or two admixed ℓ contributions.

Fig. 4 : Angular distribution of energy slices labelled in fig. 1. The curves are DWBA calculations with the contributions of different ℓ transferts. a) 2.5-8.3 MeV energy region, after substraction of the structures (see text and fig. 1). b) total slices of the high energy region (8.3-14 MeV).

Fig. 5 : Experimental and calculated fragmentation of $2d_{5/2}$ and $1g_{7/2}$ strengths in ^{207}Tl. The curves (theory) and histograms (experiment) give the strength per one MeV energy interval as a function of the separation energy. The calculation (ref. 16) includes an artificial width of 0.25 MeV. Each experimental energy scale is shifted to bring the main fragment at the right theoretical position.

Fig. 6 : Experimental and calculated fragmentation of $1g_{9/2}$ strength. The curve and histogram give the strength per one MeV energy interval. The calculation (ref.15) includes a width of 0.2 MeV. The experimental excitation energy scale is shifted by 1.25 MeV.

TABLE I - OPTICAL PARAMETERS USED IN THE ANALYSIS OF THE ^{208}Pb (d, ^{3}He)^{207} Tℓ reaction at 108 Mev

Channel		V_o (Mev)	r_o (fm)	a_o (fm)	W_v (Mev)	W_s e) (Mev)	r_i (fm)	a_i (fm)	$V_{\ell s}$ f) (Mev)	r_s (fm)	a_s (fm)	r_c fm	ReF
d		74.77	1.18	0.81	9.33	7.04	1.274	0.914				1.28	a) b)
^{3}He	set A	127.	1.14	0.83	-	28.5	1.15	0.85	-	-	-		c)
	set B = d	80.2	1.17	0.803	5.76	8.474	1.29	0.92	4.90	1.07	0.66	1.4	b)
	set B = t	54.62	1.146	0.76	3.00	7.82	1.29	0.696	6.04	1.06	0.74	-	d)
	set B = p												
P		adjusted	1.25	0.65	-	-	-	-	$\lambda \approx 25$				

a) ref. 7

b) ref. 8

c) interpolated set between 71 MeV (ref.11) and 130 MeV (ref.9) ^{3}He potentials including a pure surface imaginary term.

d) ref. 12

e) 4. x Ws is used in DWUCK 4 Code

f) 2. x Vℓs and 4. x Vℓs are respectively used for d and p.

TABLE II - $^{208}Pb(d,^{3}He)^{207}Tl$ at Ed = 108 MeV

EXPERIMENTAL SPECTROSCOPIC FACTORS OF THE VALENCE HOLE MAIN FRAGMENTS

Ex (MeV)	nlj	C^2S present work pot. A	pot. B	C^2S other works $(d,^{3}He)^{a)}$	$(t,\alpha)^{b)}$	$(\vec{t},\alpha)^{c)}$
0	3s $1/_2$	-	(1.8)	1.9	1.9	1.26
0.35	2d $3/_2$	2.7	3.8	3.4	4.6	4.35
1.34	1h $11/_2$	4.5	7.7	12.1	10.7	7.28
1.67	2d $5/_2$	2.5	3.5	4.2	3.7	3.13
3.47	1g $7/_2$	1.8	3.5	1.6	3.2	6.43

a) ref. 3 b) ref. 4 c) ref. 5

TABLE III - SPECTROSCOPIC FACTORS OF VALENCE AND INNER HOLE STATES IN ^{207}Tl

	C^2S valence holes			C^2S inner holes		
	1h $11/2$	2d $5/2$	1g $7/2$	1g $9/2$	2p	1f $5/2$
Valence main fragment	7.7	3.5	3.5	-	-	-
[2.5-7.13 Mev] Structures	0.6	1.0	3.1 (4.25[a])	0.58 (0.[a])	(0.1)	-
[2.5-7.13 Mev] Lower part	2.1	0.6	0.53 (1.42[a])	0.45 (0.[a])	(0.45)	-
[0. -7.13 Mev] total	10.4	5.1	7.13 (9.13[a])	1.03 (0.[a])	(0.55)	
[7.13-8.3 Mev] Structures	0.17	0.09	-	0.49	(0.07)	-
[7.13-8.3 Mev] lower part	0.48	0.24	-	0.8	(0.2)	-
[8.3 - 14. Mev] total	-	-	-	8.5	(3.3)	(6.)
[7.13-14. Mev] total	0.65	0.33	-	9.79	(3.57)	(6.)
[0. —14. Mev] Sum rule	92 %	91 %	89 % (115%[a])	108 % (98%[a])	(69 %)	(100 %)

a) if all ℓ=4 fragments between 5.5 and 7.13 Mev are attributed 1g 7/2

TABLE IV - FRAGMENTATION OF PROTON VALENCE AND INNER HOLE STRENGHTS IN ^{207}Tl

	This experiment				V.G. Soloviev et al.[c]			Pham Van Thieu et al.[d]		
	E_x,[ΔEX] (Mev)	$\frac{C^2S}{2J+1}$	$\overline{EX}$ (Mev)	Γ (Mev)	$\frac{C^2S}{2J+1}$	$\overline{EX}$ (Mev)	Γ (Mev)	$\frac{C^2S}{2J+1}$	$\overline{EX}$[a] (Mev)	Γ (Mev)
Valence holes			E_{SE}=8.02						E_{SE}=7.44	
$3S_{1/2}$	0.	(0.90)	0.	-	0.95	0.	-	0.9	0.	-
$2d_{3/2}$	0.35	0.95		-	0.975	0.43	-	0.95	1.05	-
$1h_{11/2}$	1.33	0.64	-	-	0.84	1.6	-	0.80	2.08	-
	[0.-8.3]	0.92	2.8	5.8	-	-	-	0.96	2.41	2.42
$2d_{5/2}$	1.67	0.58	-	-	0.77	1.9	-	0.72	2.05	-
	[0.-8.3]	0.91	3.1	5.1	-	-	-	0.91	2.71	3.52
$1g_{7/2}$	3.47	0.45	-	-	0.75	3.7	-	0.50	5.73	-
	[0.-8.3]	0.89	3.9	1.25	-	-	-	0.95	6.0	2.24
		(1.15)	(4.4)	(2.5)						
Inner holes										
$1g_{9/2}$	[5.4 -14.]	1.1 (0.98)	10.	5.0	-	-	-	0.92	10.0	3.15
	[7.25-12.25]	0.77	9.75	3.15	0.73[b]	8.0[b]	2.4[b]	-	-	-
$2p$	[4.0-14.]	(0.69)	(10.25)	(5.9)	-	-	-	-	-	-
$1f_{5/2}$	[10-14.]	(1.0)	(12.25)	(2.7)	-	-	-	-	-	-

a) excitation energies correspond to the difference of the calculated excited state and ground state separation energies (E_{SE})

b) results calculated between 6. and 11 Mev excitation energy (see fig. 6) and text.

c) Ref.15

d) Ref.16

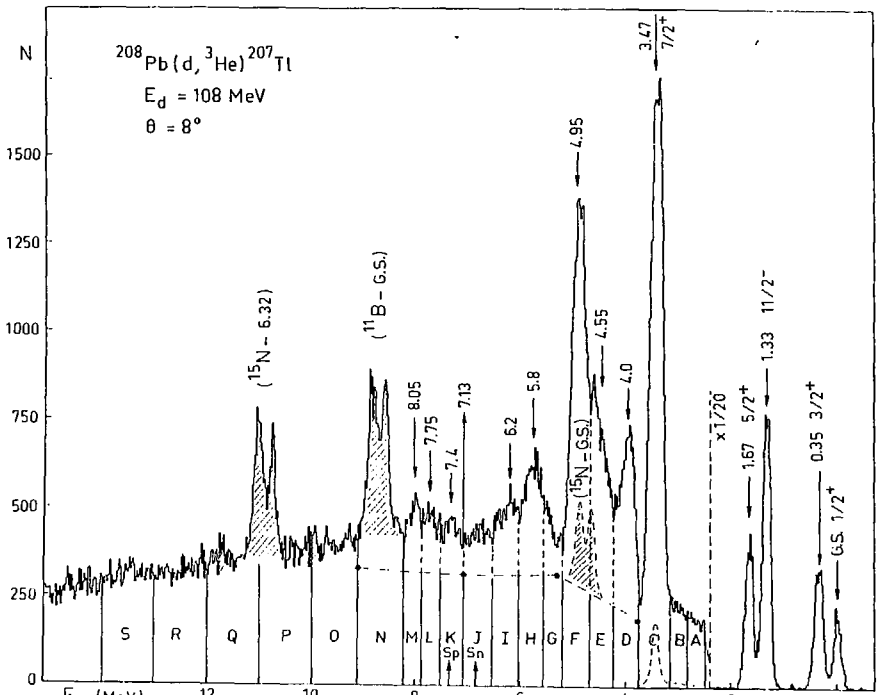
N
^{208}Pb(d, ^{3}He)^{207}Tl
E_d = 108 MeV
θ = 8°
1500
1250
1000
750
500
250
0
(^{15}N - 6.32)
(^{11}B - G.S.)
8.05
7.75
7.4
7.13
6.2
5.8
4.95
4.55
4.0
(^{15}N - G.S.)
3.47
7/2$^+$
x1/20
1.67 5/2$^+$
1.33 11/2$^-$
0.35 3/2$^+$
G.S. 1/2$^+$
S R Q P O N M L K Sp J Sn I H G F E D C B A
E_x (MeV)
12
10
8
6
4
2
0

Fig. 1

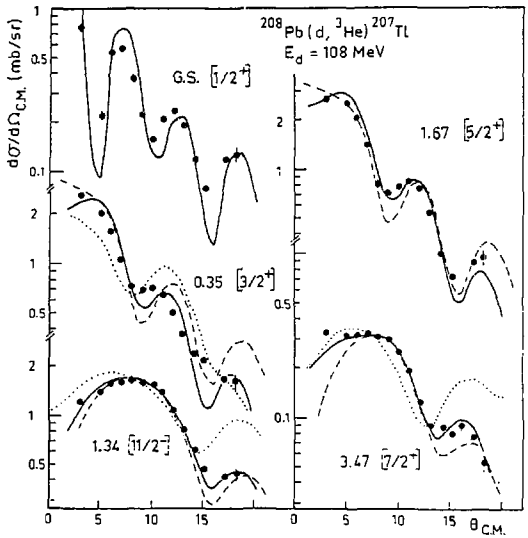
^{208}Pb(d, ^{3}He)^{207}Tl
E_d = 108 MeV
G.S. [1/2$^+$]
0.35 [3/2$^+$]
1.34 [11/2$^-$]
1.67 [5/2$^+$]
3.47 [7/2$^+$]
dσ/dΩ$_{C.M.}$ (mb/sr)
θ$_{C.M.}$

Fig. 2

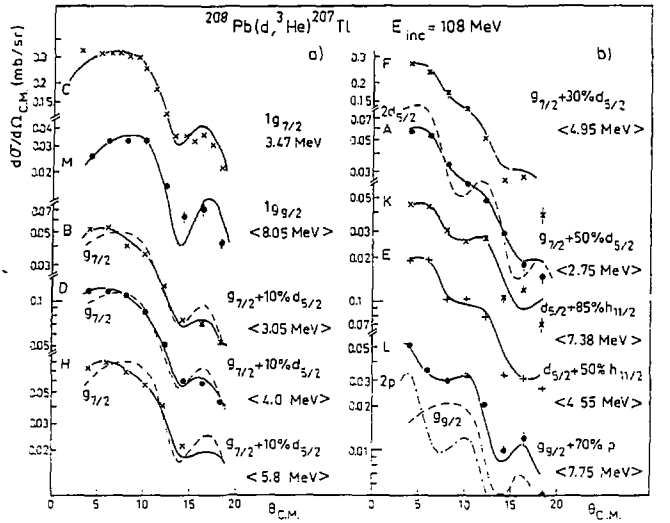
208Pb(d, 3He)207Tl
E inc = 108 MeV
a)
b)
dσ/dΩ C.M. (mb/sr)
θ C.M.
1g 7/2
3.47 MeV
1g 9/2
<8.05 MeV>
g7/2+10%d5/2
<3.05 MeV>
g7/2+10%d5/2
<4.0 MeV>
g7/2+10%d5/2
<5.8 MeV>
g7/2+30%d5/2
<4.95 MeV>
g7/2+50%d5/2
<2.75 MeV>
d5/2+85%h11/2
<7.38 MeV>
d5/2+50% h11/2
<4 55 MeV>
g9/2+70% p
<7.75 MeV>

Fig.3

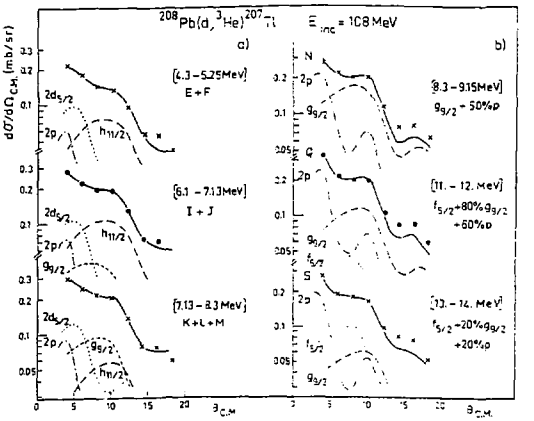
208Pb(d, 3He)207Tl
E inc = 108 MeV
a)
b)
dσ/dΩ C.M. (mb/sr)
θ C.M.
[4.3 – 5.25MeV]
E + F
[6.1 – 7.13MeV]
I + J
[7.13 – 8.3 MeV]
K + L + M
[8.3 – 9.15MeV]
g9/2 = 50%p
[11. – 12. MeV]
f5/2+80%g9/2
+60%p
[13. – 14. MeV]
f5/2 =20%g9/2
+20%p

Fig.4

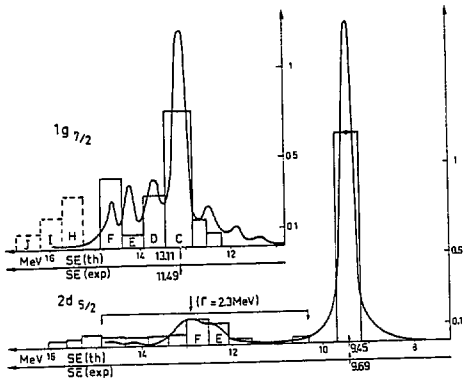
1g 7/2
J
I
H
F
E
D
C
1
0.5
0.1
MeV 16
SE(th)
SE(exp)
14
12.11
12
11.49
2d 5/2
(Γ = 2.3MeV)
F
E
1
0.5
0.1
14
12
10
9.45
8
9.69

Fig.5

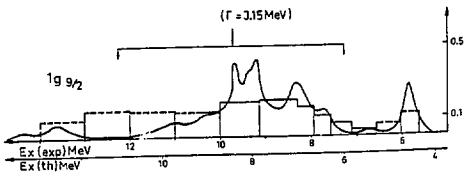
(Γ = 0.15MeV)
1g 9/2
0.5
0.1
Ex (exp) MeV
Ex (th) MeV
12
10
8
6
5
4

Fig.6